Nanoscale Advances

PAPER

View Article Online
View Journal | View Issue

Cite this: *Nanoscale Adv.*, 2019, **1**, 1035

Green biomimetic preparation of efficient Ag–ZnO heterojunctions with excellent photocatalytic performance under solar light irradiation: a novel biogenic-deposition-precipitation approach†

Manoj Kumar Choudhary,*[abd] Jyoti Kataria,[b] Vimal Kumar Bhardwaj[c] and Shweta Sharma*[d]

Herein, we report a unique single-step biogenic deposition precipitation (BDP) approach as a straightforward route for producing efficient Schottky contact between noble metal nanoparticles and wide-band-gap semiconductors. Successful preparation of Ag–ZnO heterojunctions using fennel seed extract (FSE) has been described. The effective biomolecules available in the seeds functioned as novel biogenic materials for the precipitation of adsorbed silver ions (Ag^+) on ZnO particles as metallic silver (Ag^0). The as-prepared composite materials were characterized using diffuse reflectance spectroscopy (DRS), X-ray diffraction (XRD), Fourier transform infrared spectroscopy (FT-IR), energy dispersive X-ray (EDX) study, X-ray photoelectron spectroscopy (XPS), photoluminescence spectroscopy (PL) and high-resolution transmission electron microscopy (HR-TEM). The biogenically prepared Ag–ZnO nanocomposites exhibited excellent photocatalytic activity towards reduction/degradation of colored (rhodamine B (Rh-B) dye) as well as colorless (chlorpyrifos pesticide) pollutants when irradiated under solar light. Among the prepared photocatalysts, 3 wt% Ag–ZnO hybrid composite showed the best photocatalytic activity by efficiently degrading hazardous organic pollutants within a very short time. The superior photocatalytic performance of biogenically prepared Ag–ZnO heterojunctions can be ascribed to the clean production of steady and efficient Schottky contact between plasmonic AgNPs and semiconducting ZnO NPs.

Received 31st October 2018
Accepted 20th November 2018

DOI: 10.1039/c8na00318a

rsc.li/nanoscale-advances

1. Introduction

Semiconductor-based nanomaterials, especially metal oxides (*e.g.*, ZnO, SnO_2, TiO_2, *etc.*), due to their unique potential for providing renewable energy and environmental clean-up have attracted many researchers in the recent past and captivated their interest in this field.[1–3] Among various semiconducting nanomaterials, ZnO, with a band gap (E_g) of 3.2 eV, is considered as a prospective candidate for numerous photocatalytic purposes.[1] However, due to higher magnitude of E_g, it experiences the significant drawback of recombination of photogenerated charge carriers (e^- and h^+), which results in decrease in photocatalytic efficacy. Subsequent efforts have been made in the recent past to explore optimum utilization of energy corresponding to visible region of solar spectrum.[4–6]

More recently, it has been found that plasmonic metal nanoparticles (MNPs), such as noble metals (Ag and Au), can stimulate wide-band-gap semiconductors, revealing highly extended visible light responses.[7] In simple words, on illumination with a visible light source, a strong plasmon resonance (SPR) is produced; during its dephasing, the hot excited electrons (e^-) in noble metals are injected to the conduction band (CB) of semiconductor *via* Schottky junction, leaving behind the holes (h^+) in noble metal nanoparticles.[8,9] These injected e^-s in CB of semiconductor and h^+s in MNPs are responsible for reduction and oxidation processes, respectively, at their sites.[10] This unique mechanism widens the horizons for the advancement of efficient and active photocatalysts possessing excellent visible-light activity.

There are various methods for *in situ* preparation of sub-nanometer-sized noble metal nanoparticles. One such method is the polymer pen-lithography technique.[11] Traditionally, noble metal nanoparticles are cast onto surfaces of semiconductor

[a]*Nanomaterial Research Laboratory, Department of Chemistry, Guru Nanak National College, Doraha, Ludhiana, Punjab, 141421, India. E-mail: choudhary.nrl@gmail.com; Fax: +91-1628-256731; Tel: +91-1628-257097; +91-814-6556-719*

[b]*P.G. Department of Chemistry, Panjab University Research Centre, GGDSD College, Sector 32-C, Chandigarh, 160030, India*

[c]*Department of Chemistry, Indian Institute of Technology, Rupnagar, Punjab, 140001, India*

[d]*Institute of Forensic Science and Criminology, Panjab University, Chandigarh, 160014, India. E-mail: 25shweta@pu.ac.in; Tel: +91-172-2534121; +91-987-2688-577*

† Electronic supplementary information (ESI) available. See DOI: 10.1039/c8na00318a

nanoparticles by photo-deposition (PD),[12] colloidal deposition (CD)[13] and deposition-precipitation (DP) methods.[14] Unfortunately, casting of noble metal nanoparticles onto the semiconductor surface using the lithographic technique has not yet been reported. The colloidal deposition technique involves the deposition of preformed colloidal nanoparticles onto the semiconductor surface. The organic molecules or ligands required in this procedure may deposit at the interfaces between metal particles and semiconducting material, thus forming an insulating layer, which restricts the formation of an operational Schottky junction.[15] Efforts have been made for complete removal of organic capping agents, such as extraction with suitable solvent,[16] chemical oxidation[15] or calcination.[17] The solvent extraction method is not efficient enough to eliminate all organic moieties, whereas chemical oxidation is suitable only for stable metals because it involves the use of strong oxidizing agents. Calcination is another significant approach, which involves the heating of product at a very high temperature; however, it may lead to sintering of noble metal nanoparticles or decomposition of the catalyst. Moreover, methods such as PD or DP involve exposure to ultraviolet light or use of toxic chemicals, such as $NaBH_4$, citrate or hydrazine, for the precipitation of metal particles. All these processes can cause significant risk to human beings and our environmental system. Therefore, some facile and environmentally friendly strategies are required to completely remove the use of organic capping ligands, high energy radiation, and toxic chemicals and to enable the fabrication of metal–semiconductor nanojunctions under mild conditions with enhanced visible-light activity. In this context, our research group has reported a unique green biogenic preparation approach, which made it possible to construct effective metal–semiconductor Schottky junctions with extended visible-light activity.

Here, we take the example of the fabrication of Ag–ZnO heterojunctions by treating with fennel seed extract (FSE) as a precipitating agent. Fennel is a short grown, flowering herb, which belongs to the Apiaceae family and is scientifically named as *Foeniculum vulgare*. Furthermore, the prepared Ag–ZnO composite materials were investigated for their solar light-assisted photocatalytic activity for decomposition/degradation of wastewater pollutants. A commonly used fluorescent staining dye Rhodamine B (Rh-B) and a widely used pesticide, *i.e.*, chlorpyrifos were chosen as model pollutants. The mechanism concerned with the decontamination/degradation of both pollutants is also discussed systematically. In addition, it has been observed that phytochemically prepared Ag–ZnO composites exhibit extraordinary stability and excellent photocatalytic efficacy in three consecutive reuse cycles. Thus, these biogenically prepared nanocomposite materials can be potential eco-friendly alternatives for water decontamination.

2. Materials and methods

2.1. Chemicals

ZnO nanopowder (zinc oxide; particle size <100 nm) and $AgNO_3$ (silver nitrate) were purchased from Sigma-Aldrich and RENKEM India, respectively. Rhodamine-B was obtained from Central Drug House (CDH), New Delhi, and chlorpyrifos pesticide (EC-50) was obtained from Regional Pesticide Testing Laboratory (RPTL), Chandigarh. All chemicals employed in the present research work were of analytical reagent (AR) grade and utilized as received without any further refinement. Fennel seeds (*F. vulgare*) were purchased from local suppliers in Doraha, Punjab, India. Double distilled water (DDW) was used for preparing all aqueous solutions.

2.2. Procedure for preparing aqueous fennel seed extract (FSE)

The aqueous extract of fennel seeds (FSE) was prepared as follows: a thimble made of Whatman paper, containing 5.0 g of cleaned and dried fennel seeds, was extracted for 6 h in a Soxhlet apparatus using methanol as the extracting solvent. Thereafter, methanol was evaporated using rotary evaporator and a green sticky compound was obtained, which solidified on standing for 8 h (yield = 1.26 g). Then, 500 mg (0.5 g) of this solid compound was re-dissolved in 50 mL of double distilled water and used for experiments.

2.3. Biogenic cleaner production of Ag–ZnO NP heterojunctions

The cleaner production of Ag–ZnO hybrid composite materials follows a green biogenic deposition-precipitation technique. Typically, 200 mg of ZnO powder was suspended in a test tube containing 20 mL mixture solution of water and ethanol (1 : 1 v/v, H_2O : C_2H_5OH). A silicon septum was fixed, and argon gas was purged for 15 min; then, the tube was sealed with parafilm. A calculated amount of 1 mM $AgNO_3$ solution was added dropwise through a hypodermic syringe and stirred vigorously under inert atmosphere for effective adsorption of Ag^+ ions on ZnO NP surface (deposition step). After stirring for 30 min, FSE was added through syringe and again stirred for 6 h for bio-reduction of Ag^+ to Ag^0 on to ZnO surface (precipitation step). The milky white suspension changed to dark brown during this period. Then, the mixture solution was centrifuged and washed multiple times with DDW and methanol to completely eliminate NO_3^- ions and additional phytochemicals. The obtained brown shiny powder was then dried at 80 °C for 12 h. To optimize the quantity of FSE necessary for the synthesis of AgNPs onto the ZnO surface, biosynthesis of 1 wt% Ag–ZnO nanocomposite was carried out at different mixing ratios of 1 mM $AgNO_3$ to FSE without varying other conditions (text and Fig. S1, ESI†).

2.4. Characterization of prepared photocatalysts

The diffuse reflectance spectra (DRS) in absorbance mode for bare ZnO NPs and Ag–ZnO nanocomposites were recorded using a double beam UV-visible spectrometer (model: T-90+, PG Instruments, England) equipped with integrating sphere (IS 19-1). Powder X-ray diffraction patterns were acquired over a 2θ range from 10 to 80° with incident radiation of Cu Kα (λ = 1.54 Å) using an X-ray diffractometer (PANalytical X'pert-PRO) functioning at a current of 40 mA and voltage of 45 kV. Fourier transform infrared (FT-IR) spectra with wavenumber ranging

from 4000–500 cm^{-1} were recorded using an FT-IR spectrophotometer (Nicolet-iS-50, Thermo Scientific). TEM micrographs were obtained using a high resolution transmission electron microscope (HR-TEM, G^2 20 TWIN FEI, TECNAI) operating at 200 kV. The grids were prepared by coating a drop of sonicated ethanolic solution of nanomaterials and we dried the grids before TEM observation. Elemental composition was analyzed by energy dispersive X-ray (EDX) spectroscopy. The elemental and chemical compositions were acquired using X-ray photoelectron spectroscopy (FEI, PHI 5000 Versa Probe II). Before EDX and XPS analysis, all samples were stored under vacuum for 48 h. The photoluminescence (PL) spectra were obtained at room temperature (excitation wavelength (λ_{exc}) = 350 nm) using a fluorescence spectrophotometer (LS-55, Perkin Elmer).

2.5. Photocatalytic experiment for degradation of aqueous pollutants

The photocatalytic activity of synthesized biogenic Ag–ZnO nanocomposites (1 and 3 wt% Ag–ZnO NPs) in comparison to that of bare ZnO NP powder was evaluated for degradation of Rh-B (pink colored dye) and chlorpyrifos (colorless toxic pesticide) as representative pollutants. Initially, in a photoreactor of 200 mL capacity, 100 mL Rh-B (10 μM) and photocatalyst (20 mg) were added and stirred vigorously under dark for about 30 min to achieve adsorption–desorption equilibrium. Thereafter, the mixture solution was exposed to direct sunlight. The photocatalytic degradation tests were conducted in sunny days of May 2018 between 11:00 am and 3:00 pm. To prevent heating of the reaction mixture, cold water was circulated in the outer jacket around the photoreactor. For determining the dye degradation rate, a small sample solution of around 3 mL was withdrawn after every 3 min and centrifuged to remove the catalyst. After photodegradation, the filtrate was analyzed using a UV-vis spectrophotometer to determine the Rh-B concentration in the solution. Furthermore, for degradation of chlorpyrifos, 20 mg of photocatalyst was taken with 100 mL aqueous solution of chlorpyrifos (50 ppm) in photoreactor and the procedure was identical to that used for Rh-B degradation. To analyze the pesticide degradation process, small quantity of reaction mixture was withdrawn and centrifuged and the filtrate was analyzed through a UV-vis spectrophotometer at periodic intervals of 10 min.

3. Results and discussion

3.1. Biogenic preparation and characterization of Ag–ZnO heterojunctions

Recent advancement in the preparation of hybrid materials has drawn significant attention to green, eco-friendly methods for fabrication of metal–metal oxide nanocomposites with efficient Schottky junctions for effective transport of charge carriers.[10,18] In the present study, an attempt has been made for cleaner production of Ag–ZnO hybrid composites using fennel seeds. The polyphenolic compounds present in the fennel seed extract (FSE) served as natural reducing/precipitating materials for the development of an efficient Ag–ZnO heterojunction, which proved that this protocol is a facile, cost-effective and eco-friendly approach. Scheme 1 illustrates the simple biogenic preparation procedure of Ag–ZnO NP heterojunction formation.

Fig. 1 depicts the diffuse reflectance spectra (DRS) of bare ZnO NPs and synthesized nanocomposite materials. The spectrum of bare ZnO NPs displayed an absorption band in the UV region (with wavelength around 375 nm), which indicated its inability to collect visible light. In addition, the DR spectra of Ag–ZnO hybrid composites exhibited two bands at around 375 nm and 440 nm. The broad band around 440 nm can be ascribed to surface plasmon resonance (SPR) absorption of silver (Ag^0).[19] It has been observed that on increasing the Ag content, the intensity of absorption due to SPR increases, which can be due to the increasing number of surface defects introduced during the deposition of metal atoms on

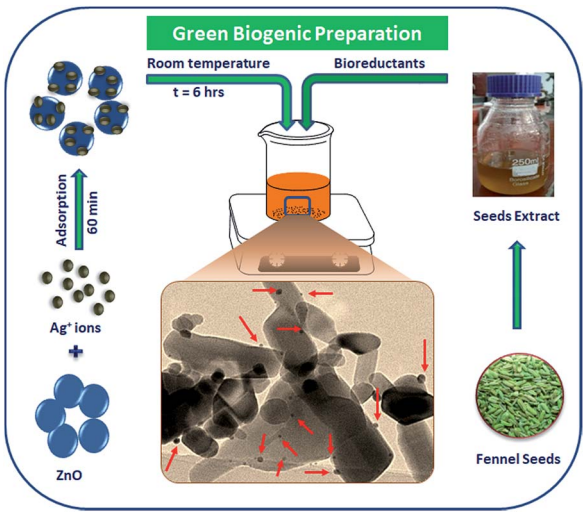

Scheme 1 Schematic illustration of the preparation procedure of Ag–ZnO nanocomposites.

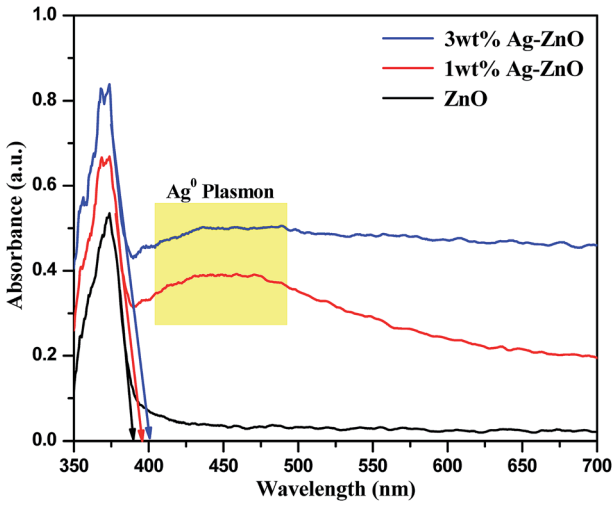

Fig. 1 DRS of bare ZnO NPs and 1 and 3 wt% Ag–ZnO hybrid composites.

semiconductors. These surface defects may limit the recombination of photoexcited e^- and h^+ pairs, thus improving photocatalytic efficacy.[20] Furthermore, ZnO NPs and synthesized Ag–ZnO hybrid materials (1 and 3 wt%) showed absorption edges (λ) at 389, 396 and 402 nm, and the corresponding observed E_g values were 3.19, 3.13 and 3.08 eV, respectively, which were calculated using an equation reported elsewhere.[21]

Bare ZnO NPs and 1 and 3 wt% Ag–ZnO composite materials were further characterized using the X-ray diffraction technique, and their corresponding XRD patterns are presented in Fig. 2. In the XRD pattern of bare ZnO NPs, all peaks matched with a standard pattern of hexagonal wurtzite structure of ZnO (JCPDS card no. 36-1451). On the other hand, both 1 and 3 wt% Ag–ZnO hybrid catalysts depicted a characteristic peak of metallic silver (marked with *) at 38.37° for the (111) plane (JCPDS card no. 04-0783). Furthermore, the prepared nanocomposites showed no shift in diffraction peaks, which indicated that the ZnO NP matrix was well preserved as the wurtzite phase. The mean crystallite sizes of ZnO NP particles calculated with the Scherrer equation were found to be similar in all samples, which further suggested that the biogenic accumulation of AgNPs does not change the crystalline structure of ZnO matrix.

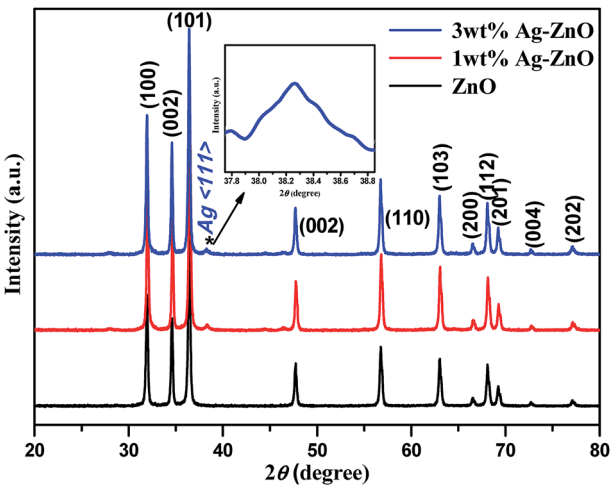

Fig. 2 XRD patterns of bare ZnO NPs and 1 and 3 wt% Ag–ZnO hybrid composites.

Fig. 3a–d depict normal transmission electron microscopy (TEM) images of Ag–ZnO nanocomposites. Uniform distribution of AgNPs was observed on ZnO surfaces without any aggregations. The size of AgNPs anchored on the surface of ZnO particles was in the range of 6–10 nm. A careful investigation of images (Fig. 3b and d) revealed that Ag and ZnO NPs were in close contact with each other, suggesting efficient formation of Schottky junction. Furthermore, HRTEM image (Fig. 3d) revealed that continuity was preserved in fringes between ZnO and AgNPs. The d-spacing of 0.27 nm in lattice fringes corresponded to the (002) plane of ZnO NPs, whereas d = 0.23 nm corresponded to the (111) plane of face centered cubic lattice structure of AgNPs. Furthermore, the qualitative and quantitative examination of silver in the biogenically prepared nanocomposites was conducted using energy dispersive X-ray

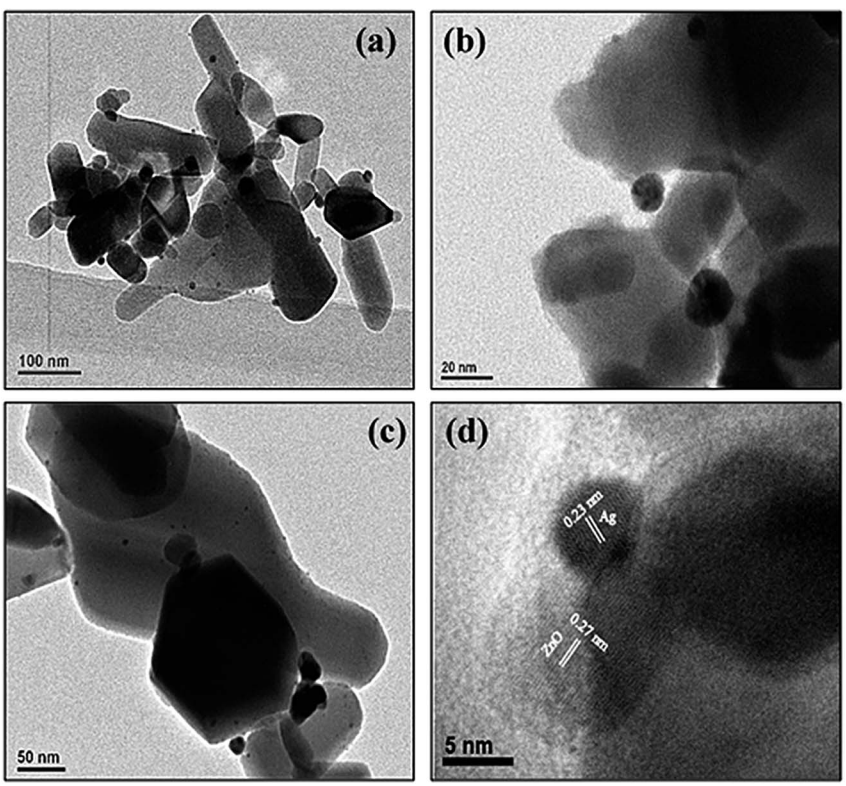

Fig. 3 TEM images (a and b) for 1 wt% Ag–ZnO and (c and d) 3 wt% Ag–ZnO.

spectroscopy (EDX) and the corresponding results are presented in Fig. S2 and S3, ESI.† The EDX spectra also reinforced the elemental constitution, as depicted in (inset) Fig. S2 and S3,† which further proved the existence of AgNPs in Ag–ZnO hybrid composite materials. It was evident from the above investigations that AgNPs were successfully deposited and precipitated on the surface of ZnO NPs by a green biogenic deposition-precipitation (BDP) route.

The elemental and chemical composition of biosynthesized 3 wt% Ag–ZnO hybrid catalyst was elucidated using X-ray photoelectron spectroscopy (XPS). The results for 3 wt% Ag–ZnO in comparison to those for bare ZnO NPs are presented in Fig. 4a. All peaks for Ag–ZnO NP photocatalysts were assigned to C, O, Zn and Ag. No peak corresponding to any element of biomolecules of fennel seeds was observed, which confirmed that biochemically fabricated Ag–ZnO catalysts were highly pure and comprised Ag, Zn and O only. These findings further supported the results obtained from EDX and XRD. Furthermore, the XPS results verified that biogenically synthesized AgNPs were successfully anchored on ZnO surfaces.

The high-resolution spectra of Zn 2p are presented in Fig. 4b. The spectra depicted two intense peaks at 1043.4 and 1020.2 eV, corresponding to binding energies of $2p_{1/2}$ and $2p_{3/2}$, which remained unchanged in bare ZnO NPs and 3 wt% Ag–ZnO hybrid composite. Also, a constant value of 23.2 eV, which is the difference between the binding energies of the two peaks ($2p_{1/2}$ and $2p_{3/2}$), confirmed that Zn existed in Zn^{2+} oxidation state in both (bare and composite) samples. In addition, high-resolution spectra of 1s orbital of oxygen for bare ZnO NPs and 3 wt% Ag–ZnO catalysts are presented in Fig. 4c. A careful observation of spectra revealed that the anchoring of Ag onto the ZnO surface did not affect the chemical nature of oxygen. A single asymmetric peak was resolved into two symmetric peaks located at 529.1 and 530.5 eV, corresponding to O 1s level of ZnO and chemically adsorbed oxygen of surface hydroxyl groups. The high-resolution spectrum of Ag 3d presented in Fig. 4d displayed two intense peaks corresponding to Ag $3d_{3/2}$ and Ag $3d_{5/2}$ levels, possessing binding energies of 372.2 and 366.2 eV, respectively. The positions of Ag 3d peaks surprisingly shifted to lower values as compared with that of bulk Ag (Ag $3d_{3/2}$, 374.2 eV and Ag $3d_{5/2}$, 368.2 eV), which suggested decrease in electron density around silver.[18] The smaller work function of Ag compared to that of ZnO NPs encouraged easy transfer of electrons from biogenically deposited plasmonic AgNPs to the

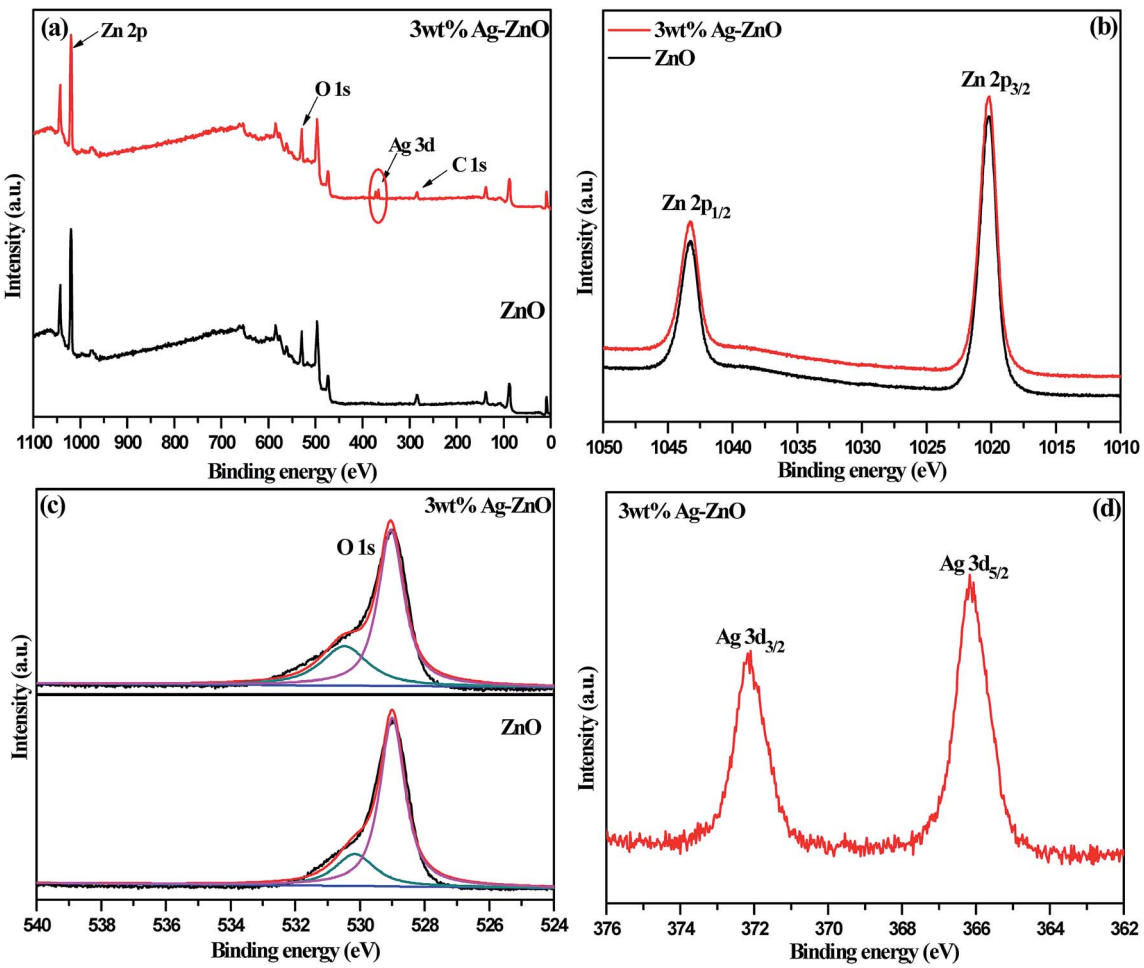

Fig. 4 (a) The complete XPS survey spectra of bare ZnO NPs and 3 wt% Ag–ZnO hybrid composite. Individual high resolution XPS spectra of (b) Zn, (c) O, and (d) Ag.

conduction band of ZnO NPs through the Schottky barrier. Thus, a new level called "Fermi level" was formed, which resulted in higher valence of silver; this further indicates efficient interparticle attraction between Ag and ZnO NPs.

The FT-IR spectra of biogenically prepared Ag–ZnO samples and bare ZnO nanopowder are displayed in Fig. 5. The vibration bands observed in the spectrum were ascribed to various lattice vibration modes. The strong band in all three spectra at 510 cm^{-1} indicated the stretching vibration of Zn–O. A broad band for ZnO NPs at 3510 cm^{-1} could be ascribed to the stretching vibration of O–H of water molecules chemisorbed onto ZnO surface. This stretching vibration slightly shifted to lower wavenumbers of 3460 and 3414 cm^{-1} for 1 and 3 wt% Ag–ZnO, respectively, due to H-bonded phenolic O–H group of polyphenolic compounds, which might be present in traces in Ag–ZnO samples. A small band at around 1420 cm^{-1} was observed in the spectra of Ag–ZnO catalysts only, which was ascribed to O–H in-plane bending vibration; a peak at 1010 cm^{-1} might be due to out-of-plane bending vibration of O–H of phenolic group.[22] Moreover, after biogenically depositing AgNPs onto the ZnO surface, the fundamental characteristic peaks for ZnO remain unchanged.

Scheme 2 depicts the plausible reaction mechanism of the preparation of nanocomposites. The active ingredients present in fennel seeds are mostly *ortho*-dihydroxy compounds such as polyphenolic acids (chlorogenic acid, rosmarinic acid, *etc.*) and flavonoids (apigenin and quercetin).[23] These dihydroxy compounds exhibit antioxidant potential;[24] they synergistically donate electrons to Ag^{+} ions adsorbed onto the ZnO nanostructures and reduce them to Ag^{0} and are concomitantly oxidized to corresponding quinones.[25,26] This BDP approach for the preparation of noble metal–metal oxide binary heterojunctions does not involve the use of any toxic chemicals or high energy input. Moreover, the entire process occurs smoothly in an aqueous solvent at room temperature; thus, it is a cost-effective and green method for nanomaterial fabrication. The biogenic preparation of Ag–ZnO nanocomposites further

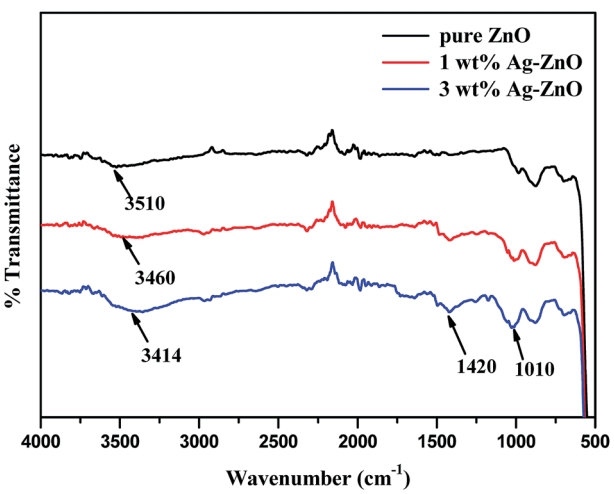

Fig. 5 FT-IR spectra of bare ZnO NPs and 1 and 3 wt% Ag–ZnO nanocomposites.

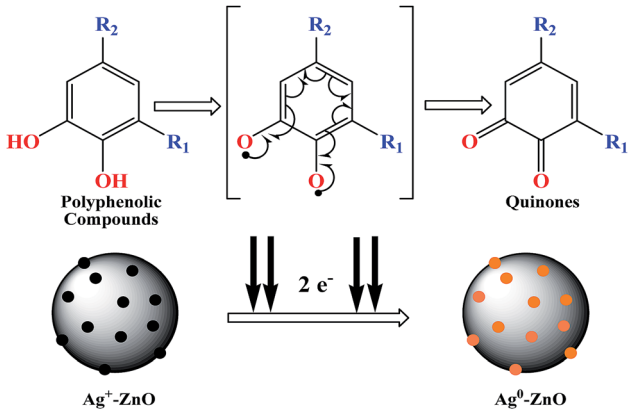

Scheme 2 Plausible reaction mechanism of formation of Ag–ZnO heterojunctions.

emphasizes the significance of this strategy for the preparation of various binary or ternary hybrid heterosystems. Another advantage is that the metal–semiconductor heterojunctions prepared using this protocol develop a strong and efficient Schottky junction, which facilitates easy transfer of charge carriers through the interface. Therefore, this ligand-free BDP approach is highly useful and shows clear superiority over other reported conventional methods for the preparation of efficient highly active materials for visible-light photocatalysis.

3.2. Photocatalytic efficacy of biogenic Ag–ZnO catalysts

The photocatalytic efficacy of biogenic Ag–ZnO catalysts (1 and 3 wt%) was examined for photodegradation of Rh-B dye and chlorpyrifos pesticide under sunlight irradiation as model photocatalytic reactions. The UV-visible spectra obtained for the photodegradation of Rh-B dye using 3 wt% Ag–ZnO, 1 wt% Ag–ZnO, and bare ZnO NPs catalysts are presented in Fig. S4a–c, (ESI†), respectively. Before illumination under sunlight, the aqueous solution of dye with each catalyst was subjected to an incubation period of dark condition for 30 min. During this period, equilibrium between adsorption and desorption processes was maintained between pollutant dye and the catalyst. Upon exposure to bright sunlight, the prominent absorption peak of Rh-B at 553 nm diminished gradually, which indicated effective dye degradation under sunlight in the presence of catalysts. In the presence of 3 wt% Ag–ZnO, complete degradation (~98.3%) of Rh-B dye was accomplished in 18 min (Fig. S4a, ESI†), whereas it degraded to ~82% in the presence of 1 wt% Ag–ZnO (Fig. S4b, ESI†). The experimental investigations shown in Fig. S4c (ESI)† reveal that in the presence of bare ZnO photocatalyst, only 68% degradation of Rh-B dye occurred in the same period, confirming the significant role of the plasmon resonance of AgNPs and fast transfer of charge carriers over the catalytic surface through Schottky junction. The kinetic curves of sunlight-driven Rh-B degradation over each catalyst are depicted in Fig. 6a and b and show that the degradation of Rh-B dye follows pseudo first order kinetics. Using 3 wt% Ag–ZnO as the catalyst, the half-life of dye was calculated using intersection between the curve of degradation efficiency ($1 - C_t/C_o$) and dye

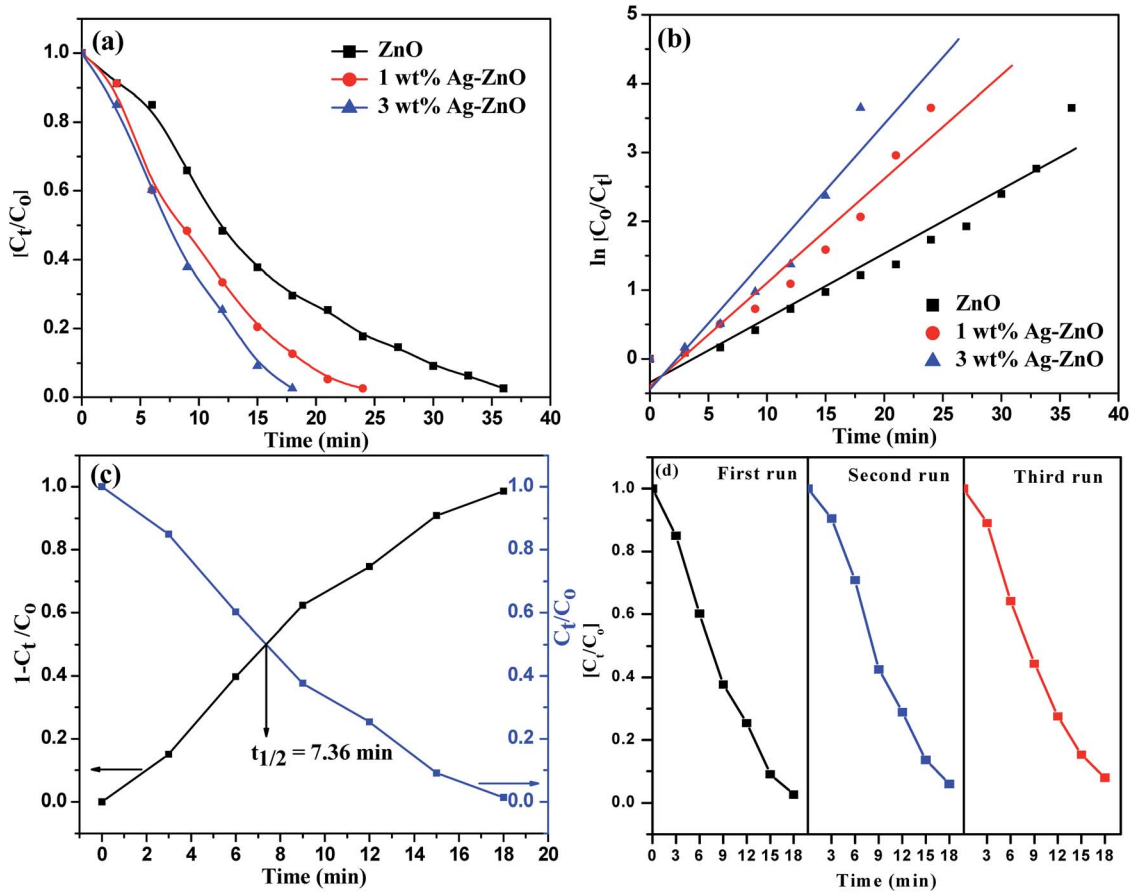

Fig. 6 (a) Comparative photocatalytic degradation of Rh-B dye using bare ZnO NPs and 1 and 3 wt% Ag–ZnO, (b) $\ln(C_o/C_t)$ *vs.* time (min) curve for photodegradation of Rh-B, (c) half-life estimation curve for degradation of Rh-B dye using 3 wt% Ag–ZnO, and (d) reusability of 3 wt% Ag–ZnO photocatalyst for decomposition of Rh-B dye for three consecutive cycles.

concentration (C_t/C_o) and it was estimated as 7.36 min (Fig. 6c). In addition to efficacy, the stability and reusability of photocatalytic materials are also significant. It is considerably relevant here because active phytoconstituents present in the *F. vulgare* seed extract may be adsorbed on the composite surface during preparation. These adsorbed phytochemicals may be degraded during photocatalysis; if phytochemicals are present, they can hinder stability and reusability. Therefore, the durability of 3 wt% Ag–ZnO hybrid was studied through repeated use. The catalyst was used in the photodegradation of dye according to the standard protocol and after the first run, the catalyst was separated from the reaction mixture by centrifugation. The recovered catalyst was then reused to degrade Rh-B in a fresh solution. Fig. 6d depicts the photocatalytic degradation of Rh-B solutions in successive three runs using a single batch of 3 wt% Ag–ZnO. No significant change in the degradation rate was observed, which indicated the high stability of prepared nanocomposites.

The UV-visible spectra of degradation of the colorless pollutant chlorpyrifos using biogenic Ag–ZnO composites as well as bare ZnO NPs are displayed in Fig. S5a–c (ESI).† To set up equilibrium between adsorption and desorption processes of pesticide molecules onto ZnO surface, the reaction mixtures with catalysts were stirred in dark for about 30 min. On exposure to bright sunlight, the absorption peak of pesticide at 293 nm decreased gradually and a new peak at around 321 nm was observed, which could be due to the formation of an intermediate product. This intermediate product further decomposed, indicating effective degradation of pesticide under sunlight in the vicinity of catalysts. In the presence of 3 wt% Ag–ZnO, ~90% degradation of pesticide was accomplished in 40 min (Fig. S5a, ESI†). With 1 wt% Ag–ZnO and bare ZnO NPs, ~75% and ~65% degradations, respectively, were observed in the same period (Fig. S5b & c, ESI†). The kinetic curves of sunlight-driven pesticide degradation over each catalyst are depicted in Fig. 7a and b, and they show that the photodegradation of pesticide follows pseudo first order kinetics. Using 3 wt% Ag–ZnO as the catalyst, the half-life of pesticide was calculated using intersection between the curve of degradation efficiency ($1 - C_t/C_o$) and dye concentration (C_t/C_o) and was estimated as 14.1 min (Fig. 7c). The above investigations of decomposition of Rh-B and chlorpyrifos reveal that 3 wt% Ag is the best precipitation amount for anchoring onto ZnO surfaces.

The photoluminescence (PL) spectra were recorded to investigate the migration of charge carriers and efficiency of recombination in Ag–ZnO hybrid composites compared to that for bare ZnO NPs. The intensity of photoluminescence is directly related to the rate of recombination of photogenerated

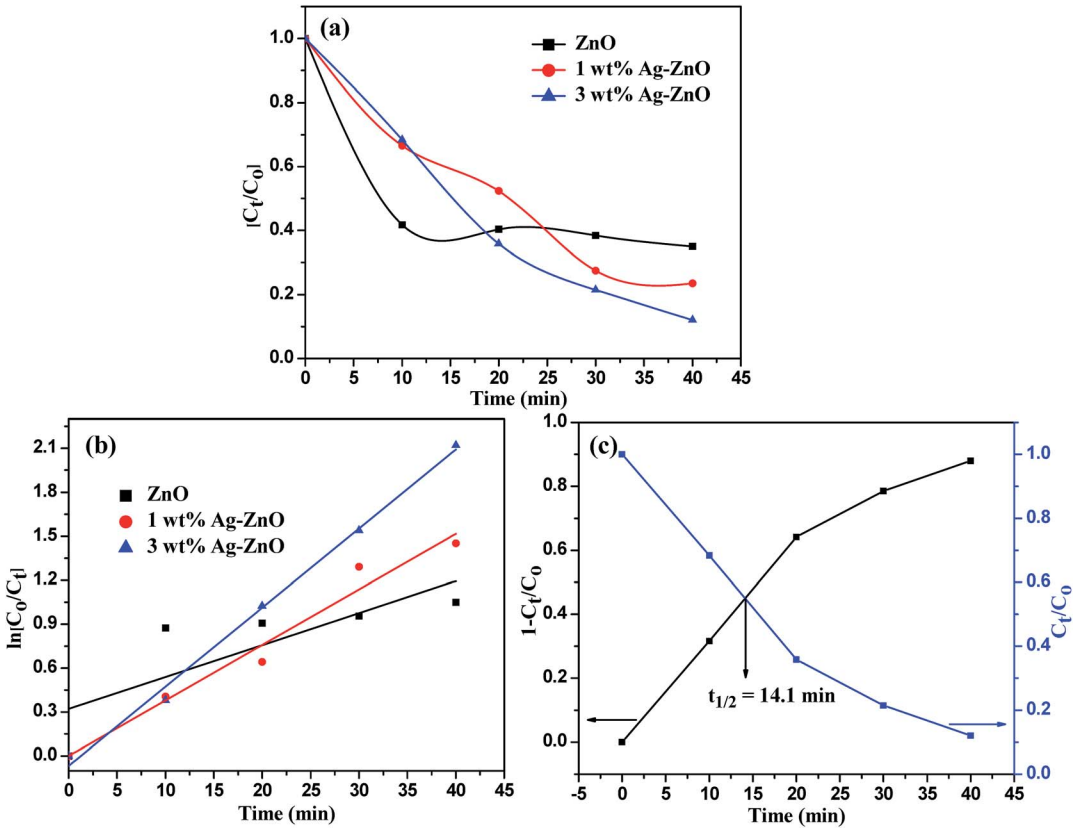

Fig. 7 (a) Comparative photocatalytic degradation of chlorpyrifos pesticide using bare ZnO NPs and 1 and 3 wt% Ag–ZnO, (b) $\ln(C_o/C_t)$ *vs.* time (min) curve for photodegradation of chlorpyrifos, and (c) half-life estimation for degradation of pesticide using 3 wt% Ag–ZnO.

e^-–h^+ pairs and inversely related to photocatalytic efficiency of semiconducting nanomaterial. Fig. 8 depicts the PL spectra of biogenically prepared Ag–ZnO nanocomposites and bare ZnO NPs analyzed at excitation wavelength (λ_{exc}) = 350 nm. The PL intensities of both nanocomposites (1 and 3 wt% Ag–ZnO) were lower than that of bare ZnO NPs, suggesting the phenomenon of Stern–Volmer quenching.[27] A decrease in PL intensity implies a lower rate of recombination of e^-–h^+ pairs and an extended lifespan of the photogenerated charge carriers.[28] The effective segregation and restriction in the recombination process of charge pairs by MNPs are promising steps for extending the photocatalytic efficacy of semiconducting nanoparticles. Therefore, it can be stated here that biogenic precipitation of silver onto ZnO nanostructures can efficiently restrict the recombination of e^-–h^+ pairs during photocatalytic reactions.

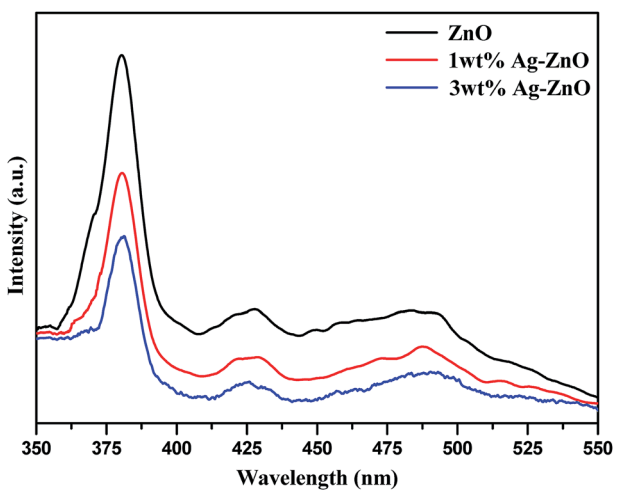

Fig. 8 PL spectra of bare ZnO NPs and 1 and 3 wt% Ag–ZnO nanocomposites.

3.3. Mechanism of photodegradation of pollutants using biogenic Ag–ZnO nanocomposites

Scheme 3 illustrates the possible mechanism of photodegradation of wastewater pollutants using biogenic Ag–ZnO nanocatalysts under solar light irradiation. The extended visible light-assisted photocatalytic competence of biogenically prepared hybrid composites (compared to that of bare ZnO nanopowder) can be elucidated because of the difference in work functions of Ag (4.2 eV) and bare ZnO NPs (5.2 eV).[29,30] It has been reported in literature that a Schottky junction is developed when two substances having considerable difference in their work functions are joined. Furthermore, the process of electron transport occurs from the substance of lower work function to that having a higher work function until both attain an equilibrium position for the creation of a Fermi level.[29,31] The equilibrated position of this new Fermi energy level generates an electric field at the boundary connecting Ag and ZnO NPs,

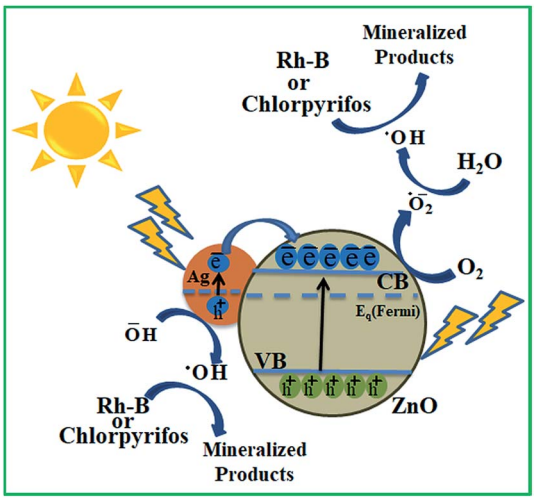

Scheme 3 Plausible mechanism for solar light-assisted photocatalytic mineralization of Rh-B and chlorpyrifos using biogenic Ag–ZnO nanocomposites.

thus enhancing the segregation of photo-excited e^-–h^+ pairs and increasing the photocatalytic efficacy.[32] On illumination under visible light, Ag–ZnO composites are excited because of SPR of metallic AgNPs and generate e^-–h^+ pairs at the NP surface. The hot excited electrons from AgNPs can transfer rapidly to CB of ZnO NPs through the interface between ZnO and AgNPs.[31,33] These relocated electrons in CB of ZnO are captured by O_2 molecules dissolved in H_2O and yield highly reactive radicals such as $^{\bullet}O_2^-$ anions and HO$^{\bullet}$ radicals.[34] The evidence of the formation of these free radicals has been reported by various research groups.[35–37] On the other side, the photo-generated holes on the AgNP surface can also be entrapped by OH^- ions and form HO$^{\bullet}$ radicals. These visible-light-generated ($^{\bullet}O_2^-$) and (HO$^{\bullet}$) radicals are extremely strong oxidative species, which are responsible for complete mineralization of hazardous pollutants.[7,18] Moreover, the photocatalytic efficiency might have constructive linkage with the degree of radical formation, *i.e.*, more rapid frequency of active radical formation causes higher photocatalytic activity of catalyst.[10,28] Overall, the experimental investigations indicate that AgNPs anchored on ZnO surfaces assist in producing highly oxidative radical species and thus accelerate efficient degradation of wastewater pollutants.

4. Conclusions

The study presented in this paper demonstrates a novel biogenic deposition-precipitation (BDP) method for the preparation of highly active Ag–ZnO photocatalysts at ambient reaction conditions using FSE without employing any toxic chemicals such as organic solvents and external chemical stabilizing agents. The development of an efficient Schottky junction at the boundary connecting AgNPs and ZnO NPs indicates that biomolecules available in FSE can be excellent materials for the preparation of hybrid photocatalysts. The fabricated Ag–ZnO catalysts exhibited exceptional photocatalytic efficacy for the mineralization of colored (Rh-B) as well as colorless (chlorpyrifos) pollutants under visible-light irradiation. Furthermore, the fennel seeds utilized in the preparation of Ag–ZnO hybrids are cheap, easily available, safe and environmentally friendly and therefore not harmful to humans and other animals in our ecosystem. In addition, the biogenic deposition-precipitation approach reported in the present research can be used in the preparation of various binary, ternary or even quaternary hybrid composite materials for different environmental or green energy-related applications.

Conflicts of interest

There are no conflicts of interest to declare.

Acknowledgements

The University Grants Commission (UGC), New Delhi, is highly acknowledged for providing financial support under minor research project scheme (F. 8-4(107)/2015(MRP/NRCB)). The authors are also thankful to the sophisticated analytical instrumentation facility at Panjab University, Chandigarh, All India Institute of Medical Science (AIIMS) – New Delhi, Indian Institute of Technology (IIT) – Kanpur and Thapar Institute of Engineering and Technology (TIET) – Patiala, for extending XRD, HR-TEM, XPS and EDX facilities, respectively.

References

1 J. Becker, K. R. Raghupathi, J. S. Pierre, D. Zhao and R. T. Koodali, *J. Phys. Chem. C*, 2011, **115**, 13844–13850.
2 A. K. Sinha, M. Pradhan, S. Sarkar and T. Pal, *Environ. Sci. Technol.*, 2013, **47**, 2339–2345.
3 X. Jiang and T. Wang, *Environ. Sci. Technol.*, 2007, **41**, 4441–4446.
4 C. Luo, D. Li, W. Wu, C. Yu, W. Li and C. Pan, *Appl. Catal., B*, 2015, **166–167**, 217–223.
5 K. Yang, Y. Zhang, C. Meng, F. F. Cao, X. Chen, X. Fu, W. Dai and C. Yu, *Appl. Surf. Sci.*, 2017, **391**, 635–644.
6 J. Wu, C. Luo, D. Li, Q. Fu and C. Pan, *J. Mater. Sci.*, 2017, **52**, 1285–1295.
7 P. Wang, B. Huang, Y. Dai and M.-H. Whangbo, *Phys. Chem. Chem. Phys.*, 2012, **14**, 9813.
8 C. Yu, G. Li, S. Kumar, H. Kawasaki and R. Jin, *J. Phys. Chem. Lett.*, 2013, **4**, 2847–2852.
9 Z. Wang, J. Liu and W. Chen, *Dalton Trans.*, 2012, **41**, 4866–4870.
10 M. K. Choudhary, J. Kataria and S. Sharma, *ACS Appl. Nano Mater.*, 2018, **1**, 1870–1878.
11 J. Wu, X. Zan, S. Li, Y. Liu, C. Cui, B. Zou, W. Zhang, H. Xu, H. Duan, D. Tian, W. Huang and F. Huo, *Nanoscale*, 2014, **6**, 749–752.
12 S. F. Chen, J. P. Li, K. Qian, W. P. Xu, Y. Lu, W. X. Huang and S. H. Yu, *Nano Res.*, 2010, **3**, 244–255.
13 D. Ding, K. Liu, S. He, C. Gao and Y. Yin, *Nano Lett.*, 2014, **14**, 6731–6736.
14 Y. Zheng, C. Chen, Y. Zhan, X. Lin, Q. Zheng, K. Wei and J. Zhu, *J. Phys. Chem. C*, 2008, **112**, 10773–10777.

15 L. Liu, S. Ouyang and J. Ye, *Angew. Chem., Int. Ed.*, 2013, **52**, 6689–6693.
16 L. D. Menard, F. Xu, R. G. Nuzzo and J. C. Yang, *J. Catal.*, 2006, **243**, 64–73.
17 M. Comotti, W.-C. Li, B. Spliethoff and F. Schüth, *J. Am. Chem. Soc.*, 2006, **128**, 917–924.
18 S. A. Ansari, M. M. Khan, M. O. Ansari, J. Lee and M. H. Cho, *J. Phys. Chem. C*, 2013, **117**, 27023–27030.
19 M. K. Choudhary, J. Kataria, S. S. Cameotra and J. Singh, *Appl. Nanosci.*, 2016, **6**, 105–111.
20 O. Bechambi, M. Chalbi, W. Najjar and S. Sayadi, *Appl. Surf. Sci.*, 2015, **347**, 414–420.
21 F. Shi, J. X. Liu, X. Huang, L. Yu, S. H. Liu, X. Feng, X. K. Wang, G. L. Shao, S. C. Hu, B. Yang and C. Y. Fan, *Adv. Powder Technol.*, 2015, **26**, 1435–1441.
22 J. Coates, *Encycl. Anal. Chem.*, 2006, pp. 1–23.
23 M. Faudale, F. Viladomat, J. Bastida, F. Poli and C. Codina, *J. Agric. Food Chem.*, 2008, **56**, 1912–1920.
24 P. C. Hugo, J. Gil-Chávez, R. R. Sotelo-Mundo, J. Namiesnik, S. Gorinstein and G. A. González-Aguilar, *Molecules*, 2012, **17**, 12657–12664.
25 M. K. Choudhary, J. Kataria and S. Sharma, *J. Cleaner Prod.*, 2018, **198**, 882–890.
26 M. K. Choudhary, J. Kataria and S. Sharma, *Appl. Nanosci.*, 2017, **7**, 439–447.
27 F. X. Redl, K.-S. Cho, C. B. Murray and S. O'Brien, *Nature*, 2003, **423**, 968–971.
28 J. Liqiang, Q. Yichun, W. Baiqi, L. Shudan, J. Baojiang, Y. Libin, F. Wei, F. Honggang and S. Jiazhong, *Sol. Energy Mater. Sol. Cells*, 2006, **90**, 1773–1787.
29 H. R. Liu, G. X. Shao, J. F. Zhao, Z. X. Zhang, Y. Zhang, J. Liang, X. G. Liu, H. S. Jia and B. S. Xu, *J. Phys. Chem. C*, 2012, **116**, 16182–16190.
30 S. S. Patil, M. G. Mali, M. S. Tamboli, D. R. Patil, M. V. Kulkarni, H. Yoon, H. Kim, S. S. Al-Deyab, S. S. Yoon, S. S. Kolekar and B. B. Kale, *Catal. Today*, 2016, **260**, 126–134.
31 Y. Liang, N. Guo, L. Li, R. Li, G. Ji and S. Gana, *New J. Chem.*, 2016, **40**, 1587–1594.
32 P. Li, Z. Wei, T. Wu, Q. Peng and Y. Li, *J. Am. Chem. Soc.*, 2011, **133**, 5660–5663.
33 H. Zhu, X. Chen, Z. Zheng, X. Ke, E. Jaatinen, J. Zhao, C. Guo, T. Xie and D. Wang, *Chem. Commun.*, 2009, 7524.
34 L. Jing, W. Zhou, G. Tian and H. Fu, *Chem. Soc. Rev.*, 2013, **42**, 9509–9549.
35 C. Hu, T. Peng, X. Hu, Y. Nie, X. Zhou, J. Qu and H. He, *J. Am. Chem. Soc.*, 2010, **132**, 857–862.
36 N. Wang, L. Shi, L. Yao, C. Lu, Y. Shi and J. Sun, *RSC Adv.*, 2018, **8**, 537–546.
37 L. Shi, J. Ma, L. Yao, L. Cui and W. Qi, *J. Colloid Interface Sci.*, 2018, **519**, 1–10.